Spectrochimica Acta Part A: Molecular and Biomolecular Spectroscopy 115 (2013) 250–258

Contents lists available at SciVerse ScienceDirect

Spectrochimica Acta Part A: Molecular and Biomolecular Spectroscopy

journal homepage: www.elsevier.com/locate/saa

Spectroscopic behavior of loratadine and desloratadine in different aqueous media conditions studied by means of TD-DFT calculations

Romina Brasca [a,b,*], Marcelo A. Romero [b,c], Héctor C. Goicoechea [a,b], Anne-Marie Kelterer [d], Walter M.F. Fabian [e]

[a] Laboratorio de Desarrollo Analítico y Quimiometría (LADAQ), Cátedra de Química Analítica I, Facultad de Bioquímica y Ciencias Biológicas, Universidad Nacional del Litoral–CONICET, Ciudad Universitaria, S3000ZAA Santa Fe, Argentina
[b] Consejo Nacional de Investigaciones Científicas y Técnicas (CONICET), Av. Rivadavia 1917, C1033AAJ Capital Federal, Argentina
[c] Instituto de Desarrollo Tecnológico para la Industria Química (INTEC-CONICET-UNL), Güemes 3450, CC91, S3000GLN Santa Fe, Argentina
[d] Institut für Physikalische und Theoretische Chemie, Technische Universität Graz, Stremayrgasse 9/I, 8010 Graz, Austria
[e] Institut für Chemie, Karl-Franzens-Universität Graz, Heinrichstraße 28, 8010 Graz, Austria

HIGHLIGHTS

- Changes in the UV spectra produced by stepwise protonation of two drugs.
- TD-DFT simulations (hybrid and long-range corrected methods) using a continuum solvation model.
- Analysis of the lowest energy transitions and molecular orbital plots.
- Potential applications of the simulated spectra in analytical chemistry.

GRAPHICAL ABSTRACT

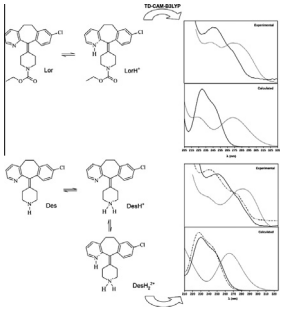

ARTICLE INFO

Article history:
Received 7 January 2013
Received in revised form 14 May 2013
Accepted 8 June 2013
Available online 19 June 2013

Keywords:
Loratadine
Desloratadine
UV spectroscopy
Time-dependent density functional calculations
Protonation

ABSTRACT

In this study, we explained the influence of the stepwise protonation of two antihistaminic drugs on their experimental absorption spectra. We demonstrated the capability of the TD-CAM-B3LYP method, combined with a polarizable continuum model, to produce good performance for the calculated spectra. The lowest energy transitions and the molecular orbital plots were analyzed in detail. The calculated UV spectra are proposed as potential alternatives to initialize the well-known MCR–ALS algorithm, especially when the spectra of the pure analytes are not available. Moreover, it can be a useful strategy for planning an experimental methodology oriented to multiway analysis when the drug species exhibit acid–base properties.

Introduction

Nowadays, the use of second-order data for the determination of pharmaceuticals in complex matrices (e.g. wastewater, drinking water, plasma, urine, fish oil, etc.) is a common practice in analytical chemistry laboratories [1]. This kind of data can be generated from hyphenated techniques (i.e. combination of chromatographic and spectral methods) [2] or excitation-emission matrices [3] and pH or kinetically modulated spectral information [4] coupled to

* Corresponding author at: Laboratorio de Desarrollo Analítico y Quimiometría (LADAQ), Cátedra de Química Analítica I, Facultad de Bioquímica y Ciencias Biológicas, Universidad Nacional del Litoral–CONICET, Ciudad Universitaria, S3000ZAA Santa Fe, Argentina. Tel.: +54 342 4575205.
E-mail address: rbrasca@fiq.unl.edu.ar (R. Brasca).

1386-1425/$ - see front matter © 2013 Elsevier B.V. All rights reserved.
http://dx.doi.org/10.1016/j.saa.2013.06.037

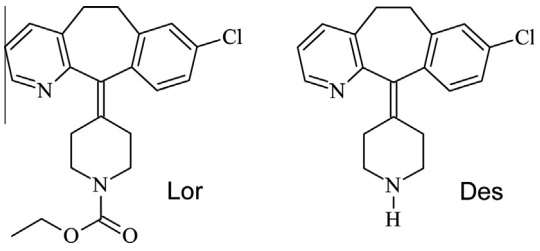

Fig. 1. Structures of loratadine (Lor) and desloratadine (Des).

multivariate calibration algorithms. The use of second-order instrumental data allows analyzing any sample containing unexpected components (interferents) in addition to the analyte of interest [5].

A common way to obtain second-order data is by implementation of a chemical reaction which involves the participation of the analyte and is monitored spectrophotometrically (i.e. reaction-based data) [6]. Another interesting methodology is to exploit the differences between the acid–base and spectral features of the drug species by means of a pH-gradient flow-injection system using a diode array spectrophotometric detector [7]. To facilitate the interpretation of the spectra, e.g. by the multivariate curve resolution–alternating least squares (MCR–ALS) method [8], additional information and/or constraints are necessary. Several methods to estimate such extra information exist, e.g. principal component analysis (PCA) [9], singular value decomposition (SVD) [10], SIMPLISMA (simple interactive self-modeling mixture analysis) [11] and EFA (evolving factor analysis) [12].

On the other hand, with the use of computational chemistry it is possible to simulate the UV spectra of the analytes. In this sense, methods based on time-dependent density functional theory (TD-DFT) [13] have been shown to provide sufficiently accurate results [14]. Therefore, we consider the use of a TD-DFT methodology as a potential alternative to initialize the MCR–ALS procedure. This alternative can be seen as a useful tool in modeling with MCR, particularly in those kinetics reactions proceeding via intermediate species which cannot be identified or isolated. We hope to apply this new concept in the near future to evaluate complex reactions of the type A + B → C; A + C → D or A → B → C by means of UV spectroscopy or drug species that display acid–base properties.

As an example for this proposed methodology here we describe the calculation of the electronic properties of two drugs, namely loratadine and its metabolite desloratadine, with acid–base character.

Loratadine is a potent tricyclic antihistaminic compound that exhibits long-lasting effects [15]. After undergoing first-pass metabolism, it is hydrolyzed to its active metabolite (desloratadine). Loratadine and desloratadine (Fig. 1) are effective in the treatment of seasonal allergic rhinitis [16] and skin disorders (e.g. chronic urticaria) [17] showing satisfactory pharmacological profiles [18].

Recently, Popovic et al. determined the pK_a values of loratadine (pK_a = 5.25) and desloratadine (pK_a = 4.41 and pK_a = 9.97 for deprotonation of the pyridinium and piperidinium rings, respectively) by means of UV–vis spectrophotometry, showing how the absorption spectrum of both drugs is modified by changing the pH of the media [19]. As a complement to this experimental investigation here we used quantum chemical methods in order to analyze the influence of the acid–base properties of these two important antihistaminic drugs on their absorption spectra.

With the goal of explaining this behavior we analyzed in detail the spectroscopic properties of both drugs in neutral and protonated forms. In order to facilitate the comparison of the computed electronic transitions with the experimental absorption bands, we recorded the UV–vis spectrum of the title compounds in water at different pH conditions.

Computational details and methodology

The geometry of both drugs was optimized in gas-phase at B3LYP/TZVP level of theory (Fig. 2) and verified as true minima by frequency calculations. Rotations around the N—C bond of the carbamate moiety in Lor as well as the axial and equatorial orientation of the H atom at the piperidine nitrogen in Des were considered. The equatorial position of the H atom in Des is more stable and only this conformation was considered for the further study.

In the Supplementary information file the coordinates for the optimized geometries (using SVP and TZVP basis sets) are given. The triple-zeta basis set optimized geometries were used thereafter

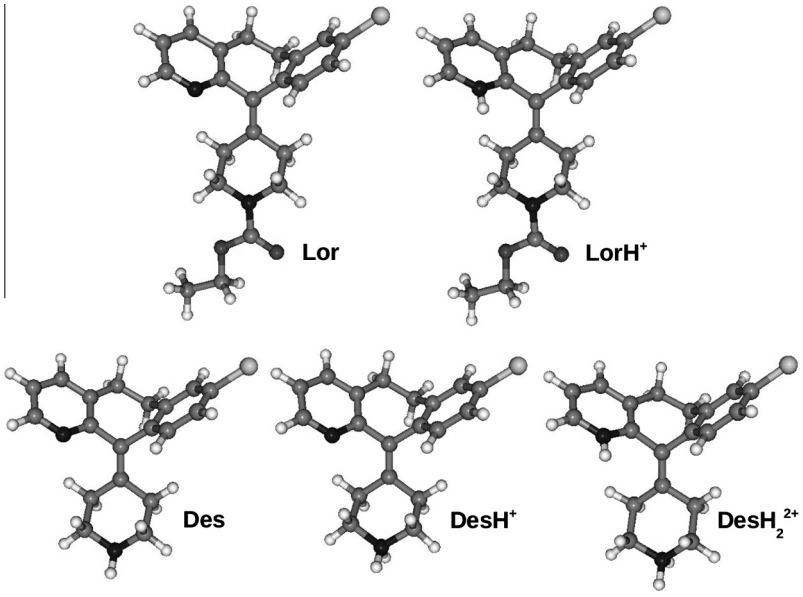

Fig. 2. B3LYP/TZVP optimized geometries of non-protonated and protonated forms of loratadine (Lor and $LorH^+$) and desloratadine (Des, $DesH^+$ and $DesH_2^{2+}$).

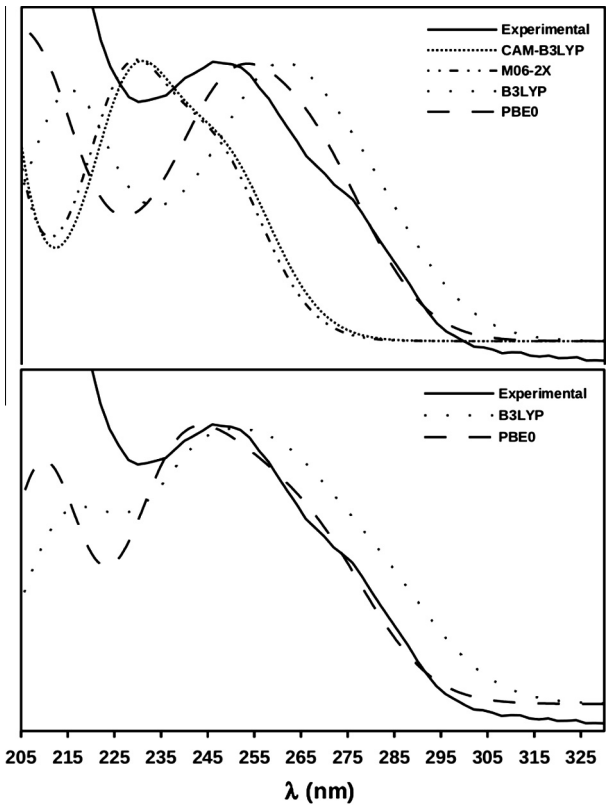

Fig. 3. Electronic spectra for non-protonated loratadine (Lor). Solvation model: CPCM (top) and COSMO (bottom).

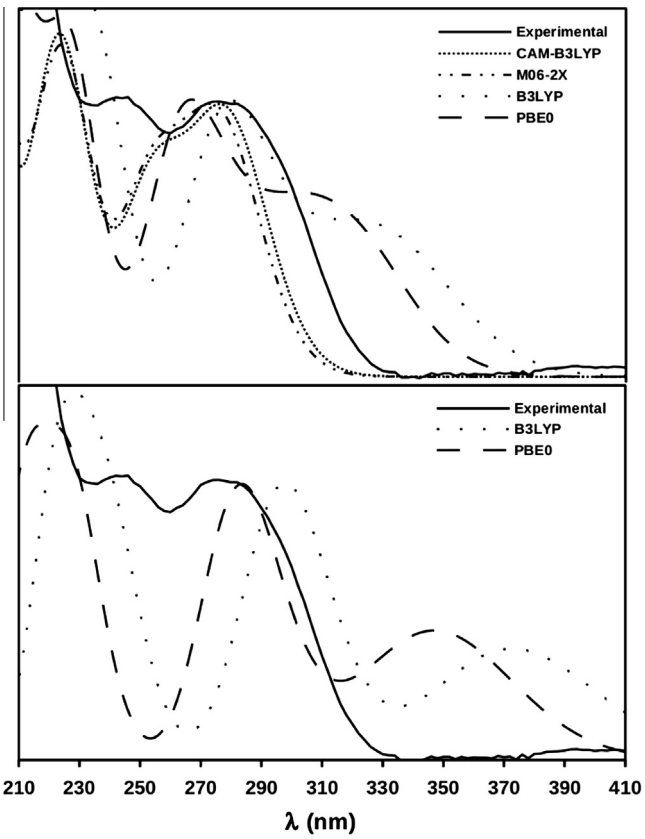

Fig. 4. Electronic spectra for protonated loratadine ($LorH^+$). Solvation model: CPCM (top) and COSMO (bottom).

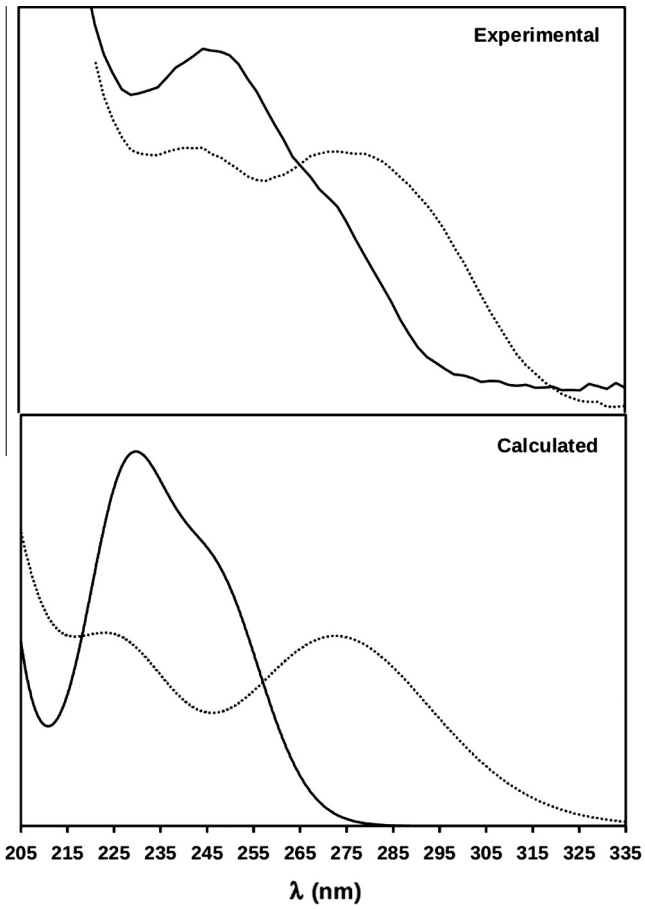

Fig. 5. Electronic spectra for non-protonated (continuous line) and protonated loratadine (dotted line). The simulations were done in water with CAM-B3LYP/TZVP.

and the data generated with the SVP geometries were only used for doing specific comparisons.

In order to have a good description of the UV properties of the compounds, we tested the performance of TD-DFT using different types of functionals (i.e. hybrid GGA, hybrid with improved long range properties and hybrid meta-GGA functionals). The following functionals were used with the TZVP [20] basis set: B3LYP [21], PBE0 [22], CAM-B3LYP [23] and M06-2X [24].

TD-DFT with the standard B3LYP and/or PBE0 is one of the most widely used methods to study UV absorption properties of organic compounds. Recently, problems in the description of Rydberg states, large π-systems and charge-transfer excited states were pointed out in conventional TD-DFT [25]. Particularly in those cases in which large-size molecules are involved, the errors regarding the vertical excitation energies and ordering of the electronic states became noticeable.

Therefore, in order to improve the behavior of the hybrid B3LYP in the asymptotic region by increasing the fraction of exact exchange, the long-range corrected (LC) functional namely CAM-B3LYP was introduced [23].

In general, LC TD-DFT methods provide an adequate description of the excited state properties of a variety of organic compounds [26].

On the other hand, Truhlar et al. recommended the use of the M11 and M06 family of density functionals for general spectroscopic applications due to the good description of ground-state properties as well as excitation energies [27].

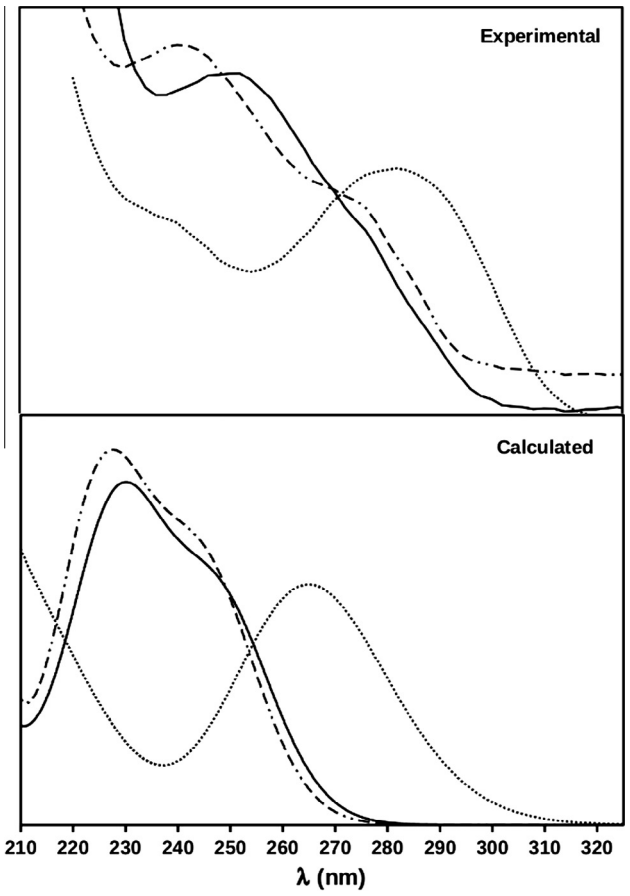

Fig. 6. Electronic spectra for non-protonated (continuous line), mono-protonated (dashed-dotted line) and di-protonated (dotted line) desloratadine. The simulations were done in water with CAM-B3LYP/TZVP.

In a very recent publication Jacquemin et al. simulated the UV spectra of twenty conjugated molecules [28]. Different effects were evaluated such as basis set, integration grid, temperature and cavities in the Polarizable Continuum Model scheme. It was shown that the functionals B3LYP, PBE0, M06, M06-2X and CAM-B3LYP provided satisfying spectra with respect to experiments.

Hence we chose besides the conventional density functionals (B3LYP, PBE0) CAM-B3LYP and M062-X.

For the organic molecules presented here the static method (TD-CAM-B3LYP/TZVP) produced results that should be good enough to make it useful in analytical chemistry applications. Nevertheless, in the cases in which static calculations are insufficient to reproduce the experimental UV spectra, the use of molecular dynamic (MD) methods is recommended [14b,29]. This kind of simulations are often required for systems in which the flexibility of the molecules is an important factor (e.g. azo dyes) and therefore, the experimental UV spectra cannot be explained taking into account only electronic effects.

Alternatively, simulations based on Boltzmann averaging can be also performed in order to produce sufficiently accurate UV–vis and CD spectra when different set of conformers are present in a molecule [30].

In the present study, the use of MD or Boltzmann-weighting simulations is not required due to the good agreement between the static results (especially the ones obtained using the SVP optimized geometries) and the experimental ones. Moreover, it would be impractical due to the enormous computational cost associated with these kind of calculations.

Calculations of vertical excitations were carried out at the ground-state SVP and TZVP-optimized geometries using an implicit solvation model. The Conductor-like Screening Model (COSMO) [31] and the Conductor-like Polarizable Continuum Model (CPCM) [32] were selected to emulate water media. The calculated electronic transitions correspond to the first 20 excitations.

Quantum chemical calculations were performed with the programs ORCA [33], Gaussian 09 [34] and GAMESS [35]. Absorption spectra were generated invoking the orca_asa program [36] using the Simple Model. For all the transitions, convolution of absorption spectra were performed by Gaussian lineshapes with a specific broadening to mimic the experimental absorption spectra.

In order to make clear comparisons, the intensities of the simulated spectra were scaled to fit those of the experimental ones.

The lambda parameter (Λ) [37], which was used as an indicator of the degree of spatial overlap between the occupied and unoccupied orbitals involved in each excitation, was computed using the program GAMESS.

Experimental details

Loratadine and desloratadine were kindly provided by Química Montpellier S.A. (Buenos Aires, Argentina). Solutions of each drug (1 ppm) were prepared in MilliQ water, hydrochloric acid and sodium hydroxide.

Absorption spectra were recorded with a Perkin Elmer Lambda 20 spectrophotometer (Waltham, Massachusetts, USA), using quartz cells with 1.00 cm path length. The spectra were recorded in the wavelength range 220–650 nm with a scan rate of 2880 nm min^{-1}. Each data point was acquired every 2 nm.

Table 1
Calculated absorption wavelengths (λ_{calc}), excitation energies (E), oscillator strengths (f), lambda parameters and assignment of the electronic transitions (ET) for loratadine.

ET	λ_{calc} (nm)	E (eV)	f	Λ	Assignment[a]	
$S_0 \rightarrow S_6$	222	5.57	0.086	0.606	H − 1 → L (25%), H → L + 3 (14%)	Lor
(State 6)	225	5.50	0.207	0.496	H → L + 1 (39%), H − 3 → L + 1 (25%)	$LorH^+$
$S_0 \rightarrow S_5$	225	5.50	0.120	0.535	H − 4 → L + 1 (26%), H − 1 → L + 1 (15%)	Lor
(State 5)	227	5.50	0.046	0.390	H − 2 → L (43%), H → L + 1 (20%)	$LorH^+$
$S_0 \rightarrow S_4$	231	5.36	0.287	0.576	H → L + 1 (28%), H − 1 → L (16%)	Lor
(State 4)	234	5.30	0.057	0.436	H − 1 → L (34%), H − 3 → L (32%)	$LorH^+$
$S_0 \rightarrow S_3$	237	5.22	0.006	0.612	H − 1 → L + 2 (27%), H − 1 → L + 1 (18%)	Lor
(State 3)	242	5.13	0.012	0.434	H − 2 → L (37%), H → L + 3 (16%)	$LorH^+$
$S_0 \rightarrow S_2$	246	5.04	0.102	0.554	H − 4 → L (34%), H − 1 → L (26%)	Lor
(State 2)	264	4.69	0.185	0.350	H − 1 → L (43%), H → L (34%)	$LorH^+$
$S_0 \rightarrow S_1$	249	4.97	0.181	0.588	H → L (58%)	Lor
(State 1)	282	4.39	0.219	0.396	H → L (48%), H − 3 → L (36%)	$LorH^+$

[a] H stands for the highest occupied molecular orbital (HOMO) and L for the lowest unoccupied molecular orbital (LUMO). The numbers in parentheses correspond to the percentage contribution of each excitation to a particular state.

Results and discussion

Choice of a suitable TD-DFT method

For the case of loratadine we checked the performance of TD-DFT calculations with five functionals and we chose the approximation that gave the best fitting with the UV experiments. In all the cases, a Gaussian lineshape with $\sigma = 1600\ cm^{-1}$ was used.

In Figs. 3 and 4 the simulated UV spectra for the neutral and protonated forms of loratadine are shown (in Fig. 1S the analogous spectra using the SVP-optimized geometries are depicted). It can be seen that the PBE0/TZVP method (COSMO model) can reproduce fairly well the spectral position of absorption maxima of loratadine (i.e. 246 nm). On the other hand, CAM-B3LYP/TZVP and M06-2X methods (CPCM model) give a good shape of the spectrum, which is blue-shifted relative to the experiment (Fig. 3).

For the case of the protonated compound (Fig. 4), two functionals are capable of reproducing the experimental spectrum in an acceptable way (i.e. CAM-B3LYP and M06-2X).

The good results obtained with both functionals are attributed to the inclusion of a high percentage of Hartree–Fock exchange (i.e. 19% HF at short-range and 65% HF at long-range for CAM-B3LYP and 54% for the hybrid meta GGA functional) [23,24].

Taking into consideration that CAM-B3LYP/TZVP is less time-consuming than M06-2X/TZVP, the former approximation was chosen for the further computations. Therefore, all the discussions

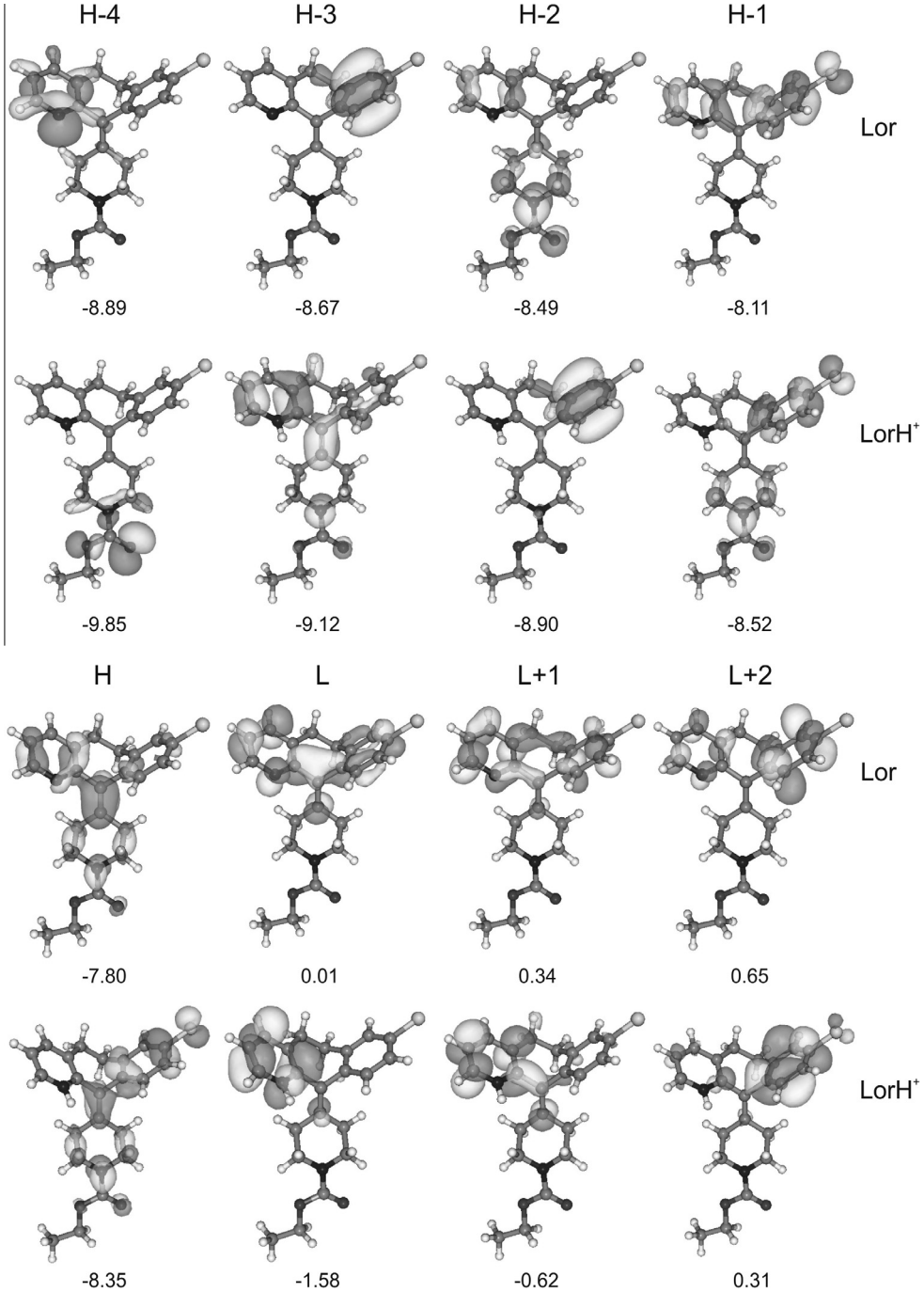

Fig. 7. Molecular orbitals involved in the lowest energy transitions of Lor and $LorH^+$. Isosurface value = 0.035 a.u.

Table 2
Calculated absorption wavelengths (λ_{calc}), excitation energies (E), oscillator strengths (f), lambda parameters and assignment of the electronic transitions (ET) for desloratadine.

ET	λ_{calc} (nm)	E (eV)	f	Λ	Assignment[a]	
$S_0 \rightarrow S_6$	222	5.57	0.098	0.587	H − 2 → L (22%), H → L + 3 (15%)	Des
(State 6)	222	5.57	0.172	0.545	H − 3 → L + 1 (27%), H − 3 → L (16%)	$DesH^+$
	218	5.70	0.142	0.670	H − 2 → L + 1 (42%), H − 3 → L (35%)	$DesH_2^{2+}$
$S_0 \rightarrow S_5$	226	5.49	0.075	0.528	H − 4 → L + 1 (30%), H − 2 → L + 1 (16%)	Des
(State 5)	223	5.55	0.074	0.645	H − 1 → L + 1 (26%), H − 1 → L (21%)	$DesH^+$
	225	5.51	0.034	0.491	H→ L + 1 (32%), H → L + 3 (24%)	$DesH_2^{2+}$
$S_0 \rightarrow S_4$	232	5.35	0.257	0.533	H → L + 1 (30%), H − 2 → L (15%)	Des
(State 4)	230	5.38	0.232	0.624	H → L + 2 (36%), H − 3 → L + 1 (23%)	$DesH^+$
	229	5.40	0.014	0.412	H → L + 1 (36%), H − 1 → L (33%)	$DesH_2^{2+}$
$S_0 \rightarrow S_3$	238	5.22	0.007	0.606	H − 2 → L + 2 (26%), H − 2 → L + 1 (17%)	Des
(State 3)	238	5.12	0.003	0.601	H − 1 → L + 2 (18%), H − 2 → L (17%)	$DesH^+$
	243	5.09	0.012	0.435	H − 1 → L (44%), H → L + 3 (14%)	$DesH_2^{2+}$
$S_0 \rightarrow S_2$	246	5.04	0.075	0.551	H − 4 → L (41%), H − 2 → L (25%)	Des
(State 2)	245	5.06	0.158	0.600	H − 1 → L (45%), H → L + 3 (14%)	$DesH^+$
	264	4.70	0.187	0.549	H − 2 → L (80%), H − 3 → L (24%)	$DesH_2^{2+}$
$S_0 \rightarrow S_1$	250	4.96	0.177	0.548	H → L (57%), H − 4 → L (14%)	Des
(State 1)	248	5.00	0.121	0.615	H → L (39%), H − 3 → L (28%)	$DesH^+$
	268	4.63	0.195	0.342	H → L (77%), H − 2 → L (10%)	$DesH_2^{2+}$

[a] H stands for the highest occupied molecular orbital (HOMO) and L for the lowest unoccupied molecular orbital (LUMO). The numbers in parentheses correspond to the percentage contribution of each excitation to a particular state.

hereafter refer to the results obtained with the CAM-B3LYP method.

In order to improve the agreement between simulated and experimental spectra, different Gaussian broadenings were used for the following spectra convolution (i.e. values in the range 1300–2200 cm^{-1}). We observed a good fitting of the simulated spectra (Figs. 5 and 6) when using $\sigma = 1500\ cm^{-1}$ for Lor, Des and $DesH^+$, whereas $2200\ cm^{-1}$ and $2000\ cm^{-1}$ were used for $LorH^+$ and $DesH_2^{2+}$, respectively.

Analysis of the main transitions

Lor and $LorH^+$

In Table 1 and Fig. 2S, the excitations in the UV region with significant oscillator strengths are shown. The main change upon protonation can be clearly seen for the states 6, 4, 2 and 1. For the protonated form the oscillator strength for state 4 is lower and that of states 6 and 2 is higher than in the case of the neutral form. Moreover, the position of the first excited states is substantially shifted to lower energy (i.e. state 1: $E = 4.97$ eV vs. $E = 4.39$ and state 2: $E = 5.04$ eV vs. $E = 4.69$).

The experimental observations upon protonation of Lor to $LorH^+$ in the absorption spectra (Fig. 5) can be explained on the basis of the previous analysis. The shoulder at ~276 nm becomes a peak and a decrease in the intensity of the peak at 246 nm is observed. This behavior can be attributed to the changes in the oscillator strengths upon protonation (for example, state 4: $f = 0.287$ vs. $f = 0.057$, see Table 1) and to the shift of the first transitions (i.e. state 1 and 2) to a longer wavelength.

In Fig. 7 the molecular orbitals (MOs) that contribute to the lowest energy transitions of both forms of loratadine are depicted. For the neutral form, the MOs involved in the observed transitions are mainly of the π–π^* type. As expected, the oscillator strength for the $n \rightarrow \pi^*$ transition (state 2: HOMO-4 → LUMO and state 5: HOMO-4 → LUMO + 1) is low for loratadine.

On the other hand, for the protonated form $LorH^+$, all the observed transitions have a π–π^* character. In this case, transitions to the pyridinium or benzene ring take part. For some states a CT character is observed (as e.g. in S1 from HOMO, located almost exclusively at the benzene moiety, to LUMO on the pyridinium ring – $\Lambda = 0.396$).

On protonation, the main change of the HOMO is observed when comparing the pyridine and pyridinium rings. The delocalization on the pyridine ring is lost upon protonation (i.e. there is no distribution over the pyridinium for the protonated form).

The main change of the LUMO is observed when comparing the benzene rings. In this case, the delocalization on the benzene moiety disappeared upon protonation.

The main difference between the occupied orbitals of both forms is that for $LorH^+$ in most of the cases there is electron distribution over the piperidine ring with contributions from the ester group. As expected, the lone-pair orbital on the nitrogen atom of the pyridine is only observed for the neutral compound and is part of the HOMO-4.

In the case of the unoccupied orbitals, in general the electronic charge is extended all over the fused tricyclic system for loratadine. On the other hand, for the protonated compound the MO delocalization is restricted either to the benzene ring or the pyridinium moiety. For example, the LUMO of $LorH^+$ is mainly localized on the pyridinium ring whereas in Lor it is distributed on the C=C fragment and on the pyridine and benzene rings as well.

Due to the protonation, all MOs are shifted to lower energies and the HOMO–LUMO gap is also diminished (from 7.81 eV to 6.77 eV).

In order to quantify the CT character of the transitions, the lambda parameter was computed at CAM-B3LYP/TZVP in water (Tables 1 and 2). An excitation with $\Lambda = 0$ corresponds to no spatial overlap (i.e. high CT character) and $\Lambda = 1$ corresponds to a local valence excitation [37]. Therefore, the lambda parameter can be used as a simple tool for measuring the CT character of the electronic transitions in the occupied-virtual orbital overlap.

The six excitations for the protonated form of loratadine exhibit smaller Λ values (i.e. 0.35–0.50) than in the case of the states of the neutral form (i.e. 0.53–0.61). This indicates that the spatial overlap between the orbitals involved in the main transitions of loratadine is higher than for protonated loratadine, in agreement with the previous discussion on the MOs. This is exemplified in Fig. 4S, in which two representative transitions for Lor (state 1) and $LorH^+$ (state 2) are shown. The different behavior of the excitations in terms of orbital overlap is evident.

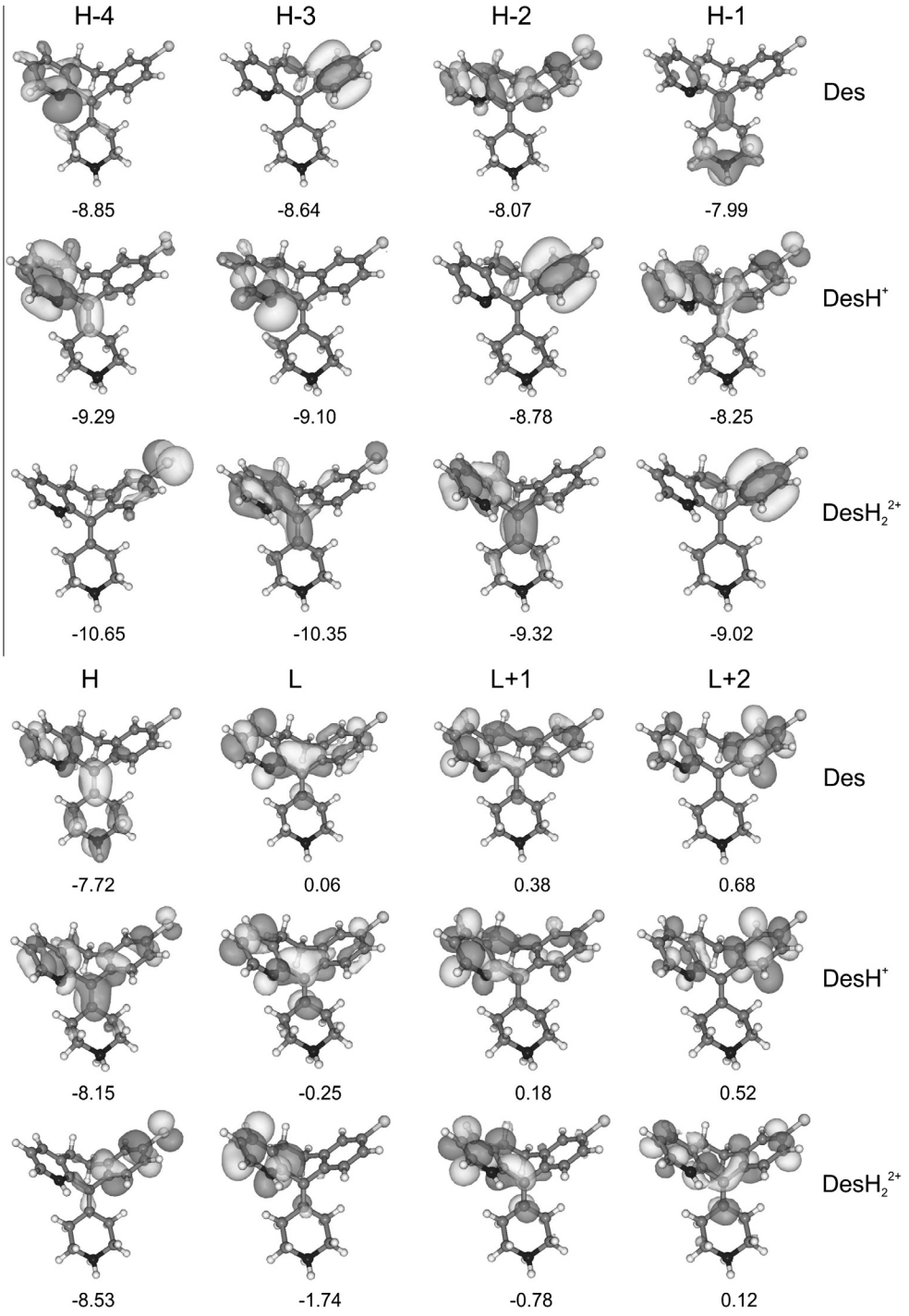

Fig. 8. Molecular orbitals involved in the lowest energy transitions of Des, $DesH^+$ and $DesH_2^{2+}$. Isosurface value = 0.035 a.u.

Des, DesH⁺ and $DesH_2^{2+}$

In Table 2 and Fig. 3S, the excitations in the UV region with large oscillator strengths are shown. The main change upon di-protonation can be clearly seen for the states 1, 2, 4 and 6. For the double protonated form the oscillator strength for state 4 is negligible and those of states 2 and 6 are higher than in the case of the neutral form. Also, the position of the first excited states is substantially shifted to lower energy (i.e. state 1: $E = 4.96$ eV vs. $E = 4.63$ and state 2: $E = 5.04$ eV vs. $E = 4.70$).

The experimental observations in the absorption spectra upon protonation (Fig. 6) can be explained on the basis of the previous analysis. Upon protonation at the piperidine ring almost no shift in the position of the main transitions can be seen. In contrast, a shift in the peak positions of ~18 nm is observed for the states 1 and 2 upon double protonation (Table 2) and changes in the oscillator strengths are noticeable for state 2, 4 and 6.

In Fig. 8 the MOs that contribute to the lowest energy transitions are depicted. For the neutral form, the MOs involved in the observed transitions are mainly of the π–π^* type. For some states a CT character is observed (e.g. the HOMO → LUMO transition has some intramolecular CT character from the piperidine ring to the fused tricyclic system – $\Lambda = 0.548$). As expected, the oscillator strength for the $n \rightarrow \pi^*$ transition (states 2 and 6) is small.

For the mono-protonated form, the oscillator strengths and positions of the peaks are very similar to the case of desloratadine because the MO distribution involved in the main transitions is not substantially modified upon mono-protonation at the piperidine moiety.

The occupied molecular orbitals are much more affected upon mono-protonation than in the case of the unoccupied orbitals. For example, upon protonation some orbitals changed their levels because the HOMO on the piperidine nitrogen disappeared (i.e. HOMO-4 in the neutral Des became the HOMO-3 in the protonated form and HOMO-3 in Des became the HOMO-2 in $DesH^+$). Moreover, the delocalization observed for the HOMO-1 in the neutral form is absent in the case of $DesH^+$.

It can be clearly seen that the LUMO delocalization is not prominent over the piperidine ring of Des and when this ring is protonated, the distribution on this part of the molecule remains unchanged.

Naturally, the characteristic lone-pair orbital on the nitrogen atom of the pyridine is absent when this ring is protonated. The pyridine lone pair is part of the lower occupied orbitals as can be seen in the HOMO-4 of Des and HOMO-3 of $DesH^+$.

For the di-protonated form, all the observed transitions have a π–π^* character. Some transitions exhibit a remarkable CT character (one example is the transition from the HOMO, located almost exclusively at the benzene moiety, to the LUMO, on the pyridinium ring – $\Lambda = 0.342$).

The unoccupied orbitals are greatly affected by di-protonation. The main change of the LUMO is observed in the benzene rings. The delocalization on the benzene moiety completely disappeared upon double protonation whereas it is not affected in the first protonation step.

The protonation of the pyridine ring increases greatly its electron attracting effect, hence the LUMO is mainly localized there and its energy drops significantly.

Upon protonation, all the MOs are shifted to lower energies. Moreover, the HOMO–LUMO gap is diminished for the double protonated form (7.78 eV for Des and 6.79 eV for $DesH_2^{2+}$).

The six excitations for the neutral and mono-protonated form of desloratadine exhibit similar Λ values (i.e. 0.53–0.61 for Des and 0.54–0.64 for $DesH^+$). In those cases, the spatial overlap between the orbitals involved in the main transitions is high. Regarding the di-protonated form, the range for lambda is 0.34–0.67, indicating a CT character for states 1, 3 and 4.

Conclusions

The main electronic transitions for loratadine and desloratadine (neutral and protonated forms) were satisfactorily analyzed using time-dependent density functional theory. For the neutral forms, the bands are mainly of the π–π^* type, and the $n \rightarrow \pi^*$ transition was also identified. For the protonated forms, especially for the fully protonated desloratadine, a remarkable CT character was observed after analyzing the lambda parameter and the MO distribution.

The computed spectra, which were generated by continuous lines approximated with Gaussian functions with adequate band shape broadening, are in accordance with the experimental results. The spectroscopic behavior that is observed upon protonation is attributed to the changes in the oscillator strengths of the main transitions and to the shift of the first transitions to longer wavelengths.

The absorption spectrum of both drugs is very similar due to the fact that the ester fragment is not involved in the main transitions. The same happened for the fully protonated compounds.

The methodology described here consists of the following steps: (a) optimization of the geometry of the drugs in gas phase; (b) SP TD-DFT computations of the vertical excitations using a proper solvation model and a suitable functional; and (c) simulation of the absorption spectra using a proper line broadening. We expect that this procedure can be extended to other pharmaceutical systems for the rational design of analytical methods, especially those that make use of the differences between the acid–base and spectral features of the drugs.

Moreover, this protocol should be extremely interesting in modeling with the well-known MCR–ALS algorithm due to the fact that the calculated UV spectra can be used to initialize the algorithm in a novel way, especially when the spectra of the pure analytes are not available. In a next publication we will show some results concerning the concrete application of the simulated spectra to the MCR–ALS initialization step in order to evaluate whether the theoretical data can be used instead of the experimental one and how well the agreement between both spectra should be.

Finally, it should be noted that the simulated UV spectra using geometries optimized with the less-demanding SVP basis set are comparable to the results from TZVP-geometries (Fig. 1S).

Acknowledgments

R. Brasca thanks CONICET for the Postdoctoral Grant and Mobility Programme.

We are grateful to Universidad Nacional del Litoral (Project CAI + D No. 12-65), CONICET (Project PIP 2988) and ANPCyT (Project PICT 2011-0005) for financial support.

Appendix A. Supplementary data

Supplementary data associated with this article can be found, in the online version, at http://dx.doi.org/10.1016/j.saa.2013.06.037.

References

[1] (a) S. Nussbaumer, P. Bonnabry, J.-L. Veuthey, S. Fleury-Souverain, Talanta 85 (2011) 2265–2289;
(b) C. Prasse, M.P. Schlsener, R. Schulz, T.A. Ternes, Environ. Sci. Technol. 44 (2010) 1728–1735;
(c) A. Checa, R. Oliver, S. Hernández-Cassou, J. Saurina, Anal. Chim. Acta 647 (2009) 1–13;
(d) M. Vosough, A. Salemi, Talanta 73 (2007) 30–36.
[2] (a) B.H. Jung, N.L. Rezk, A.S. Bridges, A.H. Corbett, A.D.M. Kashuba, Biomed. Chromatogr. 21 (2007) 1095–1104;
(b) N. Lindegardh, W. Hanpithakpong, Y. Wattanagoon, P. Singhasivanon, N.J. White, N.P.J. Day, J. Chromatogr. B 859 (2007) 74–83;
(c) S. Compain, D. Schlemmer, M. Levi, A. Pruvost, C. Goujard, J. Grassi, H. Benech, J. Mass Spectrom. 40 (2005) 9–18.
[3] (a) A. García-Reiriz, P.C. Damiani, M.J. Culzoni, H.C. Goicoechea, A.C. Olivieri, Chemom. Intell. Lab. Syst. 92 (2008) 61–70;
(b) J.M.M. Leitão, J.C.G. Esteves da Silva, A.J. Girón, A. Muñoz de la Peña, J. Fluoresc. 18 (2008) 1065–1076;
(c) I. Durán Merás, T. Galeano Díaz, M.A. Franco, Talanta 65 (2005) 7–14.
[4] (a) A. Checa, R. Oliver, J. Saurina, S. Hernández-Cassou, Anal. Chim. Acta 572 (2006) 155–164;
(b) L. Copolovici, I. Baldea, Anal. Bioanal. Chem. 374 (2002) 13–16;
(c) M.M. Reis, S.P. Gurden, A.K. Smilde, M.M.C. Ferreira, Anal. Chim. Acta 422 (2000) 21–36;
(d) A. Izquierdo-Ridorsa, J. Saurina, S. Hernández-Cassou, R. Tauler, Chemom. Intell. Lab. Syst. 38 (1997) 183–196.
[5] K.S. Booksh, B.R. Kowalski, Anal. Chem. 66 (1994). 782A–791A.
[6] J. Saurina, S. Hernández-Cassou, R. Tauler, Anal. Chem. 67 (1995) 3722–3726.
[7] (a) M.J. Culzoni, H.C. Goicoechea, Anal. Bioanal. Chem. 389 (2007) 2217–2225;
(b) A. Checa, V. González Soto, S. Hernández-Cassou, J. Saurina, Anal. Chim. Acta 554 (2005) 177–183;
(c) J. Saurina, S. Hernández-Cassou, R. Tauler, A. Izquierdo-Ridorsa, Anal. Chim. Acta 408 (2000) 135–143.
[8] (a) A. De Juan, R. Tauler, J. Chemom. 15 (2001) 749–772;
(b) R. Tauler, Chemom. Intell. Lab. Syst. 30 (1995) 133–146.
[9] (a) S. Wold, K. Esbensen, P. Geladi, Chemom. Intell. Lab. Syst. 2 (1987) 37–52;
(b) S. Wold, P. Geladi, K. Esbensen, J. Ohman, J. Chemom. 1 (1987) 41–56.

[10] E.R. Malinowski, Factor Analysis in Chemistry, third ed., Wiley, New York, 2002.
[11] W. Windig, J. Guilment, Anal. Chem. 63 (1991) 1425–1432.
[12] M. Maeder, A.D. Zuberbuhler, Anal. Chim. Acta 181 (1986) 287–291.
[13] R.E. Stratmann, G.E. Scuseria, M.J. Frisch, J. Chem. Phys. 109 (1998) 8218–8224.
[14] (a) A. Amat, S. Fantacci, F. De Angelis, B. Carlotti, F. Elisei, Theor. Chem. Acc. 131 (2012) 1218;
(b) T. De Meyer, K. Hemelsoet, L. Van der Schueren, E. Pauwels, K. De Clerck, V. Van Speybroeck, Chem. Eur. J. 18 (2012) 8120–8129;
(c) P. Gasiorski, K.S. Danel, M. Matusiewicz, T. Uchacz, W. Kuznik, L. Piatek, A.V. Kityk, Mater. Chem. Phys. 132 (2012) 330–338;
(d) A. Amat, F. Rosi, C. Miliani, A. Sgamellotti, S. Fantacci, J. Mol. Struct. 993 (2011) 43–51;
(e) A. Amat, C. Clementi, C. Miliani, A. Romani, A. Sgamellotti, S. Fantacci, Phys. Chem. Chem. Phys. 12 (2010) 6672–6684;
(f) A. Amat, C. Clementi, F. De Angelis, A. Sgamellotti, S. Fantacci, J. Phys. Chem. A 113 (2009) 15118–15126.
[15] S. Budavari, The Merck Index: An Encyclopedia of Chemicals, Drugs and Biologicals, 12th ed., Merck and Co., New Jersey, 1996. p. 953.
[16] (a) R. Anolik, Expert Opin. Drug Metab. Toxicol. 5 (2009) 683–694;
(b) C. Bachert, P. Van Cauwenberge, Clin. Ther. 29 (2007) 1795–1802;
(c) L.E. Mansfield, Expert Opin. Pharmacother. 7 (2006) 941–951;
(d) G. Passalacqua, G.W. Canonica, Clin. Ther. 27 (2005) 979–992;
(e) F.E. Simons, B.M. Prenner, A. Finn Jr., J. Allergy Clin. Immunol. 111 (2003) 617–622;
(f) R.S. Geha, E.O. Meltzer, J. Allergy Clin. Immunol. 107 (2001) 751–762.
[17] (a) M. Staevska, T.A. Popov, T. Kralimarkova, C. Lazarova, S. Kraeva, D. Popova, D.S. Church, V. Dimitrov, M.K. Church, J. Allergy Clin. Immunol. 125 (2010) 676–682;
(b) M. Haria, A. Fitton, D.H. Peters, Drugs 48 (1994) 617–637;
(c) B. Belaich, D. Bruttmann, H. DeGreef, Ann. Allergy 64 (1990) 191–194.
[18] (a) A. Banerji, A.A. Long, C.A. Camargo Jr., Allergy Asthma Proc. 28 (2007) 418–426;
(b) L. Limon, D.R. Kockler, Ann. Pharmacother. 37 (2003) 237–246;
(c) G.M. Walsh, Am. J. Respir. Med. 1 (2002) 27–34;
(d) K. McClellan, B. Jarvis, Drugs 61 (2001) 789–796;
(e) A. Graul, P.A. Leeson, J. Castaoer, Drug Future 25 (2000) 339–346;
(f) J.N. Delgado, W.A. Remers, Wilson and Gisvold's Text book of Organic Medicinal and Pharmaceutical Chemistry, ninth ed., Lippincott-Raven, New York, 1991.
[19] G. Popovic, M. Cakar, D. Agbaba, J. Pharm. Biomed. Anal. 49 (2009) 42–47.
[20] (a) A. Schafer, C. Huber, R. Ahlrichs, J. Chem. Phys. 100 (1994) 5829–5835;
(b) A. Schaefer, H. Horn, R. Ahlrichs, J. Chem. Phys. 97 (1992) 2571–2577.
[21] A.D. Becke, J. Chem. Phys. 98 (1993) 5648–5652.
[22] (a) C. Adamo, V. Barone, J. Chem. Phys. 110 (1999) 6158–6169;
(b) J.P. Perdew, K. Burke, M. Ernzerhof, Phys. Rev. Lett. 77 (1996) 3865–3868.
[23] T. Yanai, D. Tew, N. Handy, Chem. Phys. Lett. 393 (2004) 51–57.
[24] Y. Zhao, D.G. Truhlar, Theor. Chem. Acc. 120 (2008) 215–241.
[25] (a) B.M. Wong, T.H. Hsieh, J. Chem. Theory Comput. 6 (2010) 3704–3712;
(b) S. Grimme, M. Parac, Chem. Phys. Chem. 3 (2003) 292–295;
(c) B.M. Wong, J.G. Cordaro, J. Chem. Phys. 129 (2008). 214703-1–214703-8;
(d) T. Stein, L. Kronik, R. Baer, J. Am. Chem. Soc. 131 (2009) 2818–2820;
(e) B.M. Wong, M. Piacenza, F. Della Sala, Phys. Chem. Chem. Phys. 11 (2009) 4498–4508;
(f) A. Dreuw, M. Head-Gordon, J. Am. Chem. Soc. 126 (2004) 4007–4016.
[26] (a) A.D. Laurent, D. Jacquemin, Int. J. Quantum Chem. (2013), http://dx.doi.org/10.1002/qua.24438;
(b) A.V. Kityk, J. Phys. Chem. A 116 (2012) 3048–3055;
(c) M.E. Foster, B.M. Wong, J. Chem. Theory Comput. 8 (2012) 2682–2687;
(d) M. Pastore, S. Fantacci, F. De Angelis, J. Phys. Chem. C 114 (2010) 22742–22750;
(e) A.D. Dwyer, D.J. Tozer, Phys. Chem. Chem. Phys. 12 (2010) 2816–2818;
(f) T.S. Kuhlman, K.V. Mikkelsen, K.B. Møller, T.I. Sølling, Chem. Phys. Lett. 478 (2009) 127–131.
[27] (a) R. Peverati, D.G. Truhlar, Phys. Chem. Chem. Phys. 14 (2012) 11363–11370;
(b) D. Jacquemin, Y. Zhao, R. Valero, C. Adamo, I. Ciofini, D.G. Truhlar, J. Chem. Theory Comput. 8 (2012) 1255–1259;
(c) R. Li, J. Zheng, D.G. Truhlar, Phys. Chem. Chem. Phys. 12 (2010) 12697–12701;
(d) D. Jacquemin, E.A. Perpète, I. Ciofini, C. Adamo, R. Valero, Y. Zhao, D.G. Truhlar, J. Chem. Theory Comput. 6 (2010) 2071–2085;
(e) Y. Zhao, D.G. Truhlar, J. Phys. Chem. A 110 (2006) 13126–13130.
[28] A. Charaf-Eddin, A. Planchat, B. Mennucci, C. Adamo, D. Jacquemin, J. Chem. Theory Comput. 9 (2013) 2749–2760.
[29] T. Etienne, T. Very, E.A. Perpète, A. Monari, X. Assfeld, J. Phys. Chem. B 117 (2013) 4973–4980.
[30] (a) G. Uray, U.G. Wagner, W.M.F. Fabian, Comp. Theor. Chem. 977 (2011) 103–110;
(b) Y. Nakai, M. Nishizaka, C. Yang, G. Fukuhara, T. Mori, Y. Inoue, Chirality 23 (2011). E22–E27;
(c) M. Nishizaka, T. Mori, Y. Inoue, J. Phys. Chem. A 115 (2011) 5488–5495;
(d) T. Mori, Y. Inoue, S. Grimme, J. Phys. Chem. A 111 (2007) 4222–4234.
[31] S. Sinnecker, A. Rajendran, A. Klamt, M. Diedenhofen, F. Neese, J. Phys. Chem. A 110 (2006) 2235–2245.
[32] (a) A. Klamt, V. Jonas, T. Buerger, J.C.W. Lohrenz, J. Phys. Chem. A 102 (1998) 5074–5085;
(b) J. Tomasi, M. Persico, Chem. Rev. 94 (1994) 2027–2094;
(c) A. Klamt, G. Schüürmann, J. Chem. Soc. Perkin Trans. 2 (1993) 799–805.
[33] F. Neese, F. Wennmohs et al., ORCA: An Ab Initio, DFT and Semiempirical SCF-MO Package, Version 2.8, University Bonn, Bonn, Germany, September 2010.
[34] M.J. Frisch et al., Gaussian 09, Revision A.02, Gaussian, Inc., Wallingford, CT, 2009.
[35] M.W. Schmidt, K.K. Baldridge, J.A. Boatz, S.T. Elbert, M.S. Gordon, J.H. Jensen, S. Koseki, N. Matsunaga, K.A. Nguyen, S. Su, T.L. Windus, M. Dupuis, J.A. Montgomery, J. Comput. Chem. 14 (1993) 1347–1363.
[36] (a) T. Petrenko, F. Neese, ORCA_ASA, Version 2.6.35, University of Bonn, Bonn, Germany, 2008;
(b) T. Petrenko, F. Neese, J. Chem. Phys. 127 (2007) 164319–164324.
[37] (a) M.J.G. Peach, C.R. Le Sueur, K. Ruud, M. Guillaume, D.J. Tozer, Phys. Chem. Chem. Phys. 11 (2009) 4465–4470;
(b) M.J. Peach, P. Benfield, T. Helgaker, D.J. Tozer, J. Chem. Phys. 128 (2008). 044118-1–044118-8.